Journal of Studies in Science and Engineering

EngiScience Publisher

Research Article

The Initial Estimation of Anthropogenic Heat Emission in Cairo, Depending on the Inventory Approach

Shimaa Saadeldin [1,*], Ahmed Fekry [1], Abbas Mohamed El-Zafarany [2]

[1] Architecture Department, Faculty of Engineering, Cairo University, Cairo, 12613, Egypt

[2] Urban Design Department, Faculty of Urban and Regional Planning, Cairo University, Cairo, 12613, Egypt

*Corresponding Author: Shimaa Saadeldin, E-mail: shimaa.abdelmagied87@eng1.cu.edu.eg

Article Info

Article History

Received May 25, 2024

Revised Aug 13, 2024

Accepted Aug 17, 2024

Keywords

Anthropogenic heat

Urban heat island

Cairo

Inventory approach

Cairo's hotspots

Abstract

Cairo in Egypt is one of the megacities that suffer from the Urban Heat Island (UHI) phenomenon because of its high population, lack of greens, use of traditional materials and anthropogenic heat flux (AHF). The present study aimed to estimate AHF in Cairo for 2010, 2015 and 2020, depending on the energy inventory approach. The results showed that the average anthropogenic heat was 28.4 w/m^2, 24.45 w/m^2 and 21.96 w/m^2 in 2010, 2015 and 2020, respectively. Vehicles were the main cause, followed by buildings, metabolism and industry. AHF per capita share was 1803.21 w/m^2, 1514.7 w/m^2 and 1313.45 w/m^2 during the years of the study. Depending on Cairo's population data from CAMPAS and the estimated area, the hotspots were detected in Bāb ash-Sha'riyah and Al-Mūskī. The study further found that the average AHF in Cairo decreased due to GDP and the decline in per capita share and that if the consumed energy rates and gross domestic product (GDP) were within the global averages, AHF would have increased by 40%–43%. Understanding AHF patterns and causal weights is crucial for urban planning to manage AHF hotspots, to ensure people's health by maximizing thermal comfort impacts, and to plan future interventions to reduce AHF..

1. Introduction

UHI's expression was known in a study in London [1] and discussed in several studies [2–10]. The UHI phenomenon is defined as the difference in temperature between urban and non-urban areas. This difference results from the urban structure, city size, location, climate, and anthropogenic heat [11, 12].

AHF [13], as one of UHI's causes, is defined as the released heat from human activities; it is measured per unit time and unit area [14]. Eaton estimated anthropogenic heat, or artificial heat, for the first time in 1877 [15], who tried to quantify the released heat from human activities in crowded areas in London and found that it raised the air temperature by 1.4°C. The relationship between AHF and UHI was studied previously. In Hangzhou, China [16], AHF was 43.6% and 54.5% of the UHI in the summer and the winter,

respectively. In Houston, AHF was 43% of the solar re-radiation in the summer and 34% in the winter [17]. In Berlin in 1965, the contribution of the AHF to solar re-radiation was one-third, and in Vienna, it ranged from one-sixth to one-third [15].

AHF's presence was documented in the studies listed in Table 1. The sources of AHF were metabolism, vehicles, industry, and buildings [24]. The relative importance of each component varied according to GDP [25], which reflects the level of the community's welfare.

Table 1. AHF's presence in the world

Location	Year	AHF Presence	
Europe	2005	It ranged between 0.7–3.6 watt\m^2.	[18]
Beijing, China	2012	It was 135 w/m^2 in the winter and 77 w/m^2 in the summer.	[19]
Angul-Talcher, India	1993	The average was 10 w/m^2, 70 w/m^2 in hotspots, and 401.47w/m^2 in the industrial area	[20]
Toulouse, France	2005	It was 70 w/m^2 in the winter and 15 w/m^2 in the summer.	[21]
Manchester	2003	The average was 6.12 w/m^2 and was 23 w/m^2 in the high-density area.	[22]
London	1971–1979	The average was 11 w/m^2, and the maximum was 13.8 w/m^2	[23]
London	2005–2008	The average was 9 w/m^2, and the average from 2005–2008 was 10.9 w/m$^{2.}$	

- Buildings: This is an important component in forming AHF. The consumed energy in buildings worldwide is one-fifth of the total consumed energy, and this share increases by 1.3% per year [26]. In Singapore, buildings' AHF formed approximately 9% of the net radiation [26]. In Tokyo, the generated heat from air conditioning units raised the air temperature by 1℃ to 2℃ [27]. In Manchester in 2003, the percentage of the released heat from buildings was 60% [22].
- Vehicles: Most estimation processes depend on data availability, and every study has its estimation method. In Lodz, Poland [28], the authors used annual sales of petrol and diesel and multiplied them by the proportion of the population living in urban areas. In Tokyo in 1994 [29], the authors divided annual energy use by season and hour, assuming the traffic density was spatially uniform across the study area. The vehicles formed 32% and 30% of the AHF in Manchester [22] and Beijing, China [19].
- Metabolism: This is the heat released from bodies due to their activities. The sources of metabolism are divided into animals (the neglected one) and humans (the dominant one) [24]. As reported in several studies [13, 47, 48], AHF concentration is proportional to population density. In the United States, metabolism is shared by 2%–3% of the total AHF [13, 24]. In contrast, several studies neglected the metabolism shared percentage, which did not exceed 1% of the city's total AHF [30]. In Manchester [22], Tokyo [31], and Beijing [19], the metabolism formed 8%, 5%–10%, and 5% of the UHI, respectively.
- Industry: This caused 20% of the total AHF in Beijing, China [19]. Most studies neglect this source because it is located outside the city.

Estimating AHF depends on the available data and the required outputs. There are three classical approaches, as well as the urban simulation approach. The methods [24] are as follows:

1. The oldest method [15], a statistical regression method [31], is called the inventory approach or top-down approach [30]. This approach depends on relatively coarse data from governmental sources (metabolism, industry, vehicles and buildings) [13]. This approach is the most widely used and standardized [22, 28, 31–34]. We can implement this method by using Equation (1), where (Q_F) is AHF; (Q_B), (Q_V), (Q_M), and (Q_I) are the amount of heat released from buildings, vehicles, population, and industrial activities, respectively.

$$Q_F = Q_B + Q_V + Q_M + Q_I \quad (1)$$

2. The energy-budget residual approach, also called the energy budget approach, has been used in a few studies [33, 37–39]. This approach relies on tracking an urban space's energy balance factors, satellite remote sensing, and ground meteorological data. AHF can be quantified by applying Equation (2) [13], where Q_F is AHF, Q_H is the sensible heat, Q_E is the latent heat, ΔQ_S is the soil heat flux, and Q* is the net radiation.

$$Q_F = Q_H + Q_E + \Delta Q_S - Q* \quad (2)$$

3. The bottom-up approach [30], also called the GIS modelling approach [37], or the building energy models method [13], in contrast to the inventory approach, starts from the bottom of the building sector. This method relies on collecting the prototype building's data from GIS maps, such as the building's age, type, volume and area, and then integrating the simulated results [37].
4. The urban simulation approach is an extension of the GIS method. This method depends on simulation applications, such as LUCY [38], DMA [19], NJU-RBLM model, and ARPS model [39]. Several studies have depended on this approach [19, 20, 29, 41].

Megacities are defined as cities that have a population of more than 10 million people [40]. These cities are home to 6.7% of the world's population, so more energy use and AHF are concentrated in these cities. In calculations of the AHF for megacities, the largest AHF was in Seoul (76 w/m^2), the least from Karachi (6 w/m^2), and Cairo was the 23rd [46].

Cairo, a megacity with a population of more than 10 million, was the 25th in global power consumption [40]. With one of the biggest urban agglomerations in Africa [46], Cairo suffers from the UHI phenomenon [12, 41–43] and therefore from AHF. In 2010, AHF in Cairo was 10 w/m^2 [40]. This rate was divided into 51% for the industrial and residential energy use sectors, 4% for vehicle use, 22% for

electricity, and 23% for metabolism. In a study evaluating the effect of AHF on pedestrian thermal comfort in AL Hussain square [47], the air conditioning compressors raised air temperature to 1℃ when they were than three meters from the ground floor surface, and the idling buses increased the air temperature by 1℃ to 4℃ based on air velocity.

Evidence in existing literature suggested that AHF in Cairo was scarce and made an overall estimation. In addition, those studies did not discuss the effect of every cause separately (vehicles, buildings, industry and metabolism) to find the main sources of AHF. The study responded to several questions, which can be summarized as, "Is there anthropogenic heat in Cairo?" And if there is, where are the main hotspots? The main objective of this study was to estimate the anthropogenic heat in Cairo preliminarily and to assess the relative weight of each cause so that the effect can be minimized. The study focused on 2010, 2015, and 2020 because they provided a recent image of AHF and its causes in Cairo based on recent economic and urban fluctuation. The results will contribute to evaluating the city's economic and urban planning decisions during the upcoming period.

2. Methodology

2.1. Study Area

The administrative borders of Cairo are shown in Figure 1. From northwest Cairo, surrounded by Al Qalyubia and Al Giza; from the west, south and east, surrounded by the desert. According to Köppen, 1884, Cairo's climate classification is hot and arid [46, 49]. Cairo's role as the capital city results in mixed activities and land use. The city's population density varies [43], with some areas being highly populated and others less. The total area is 3,085 km², but more than half of this area is desert and planned but uninhabited. AHF is generated from human activities, so if its calculations depend on the total area, the results will not reflect the actual situation. This study focuses only on Cairo's urban areas.

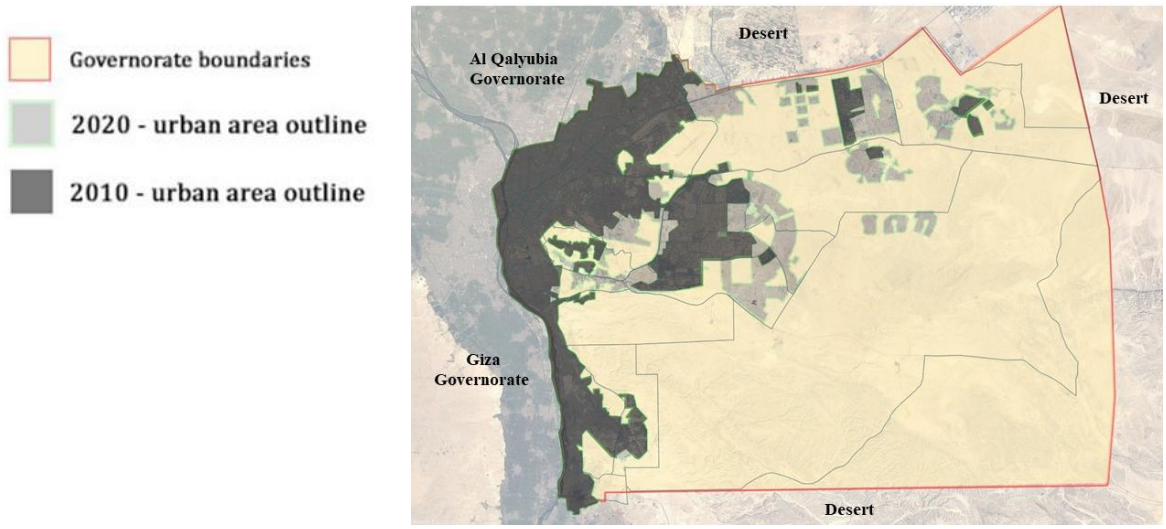

Figure 1. Cairo's governorate borders and urbanization are expanding (Authors)

Several techniques were processed to detect and calculate the urban areas and the land use/land cover change over 2010, 2015 and 2020. Data were collected from Landsat 8 imagery and ancillary (for 2015 and 2020) and Landsat 7 imagery and ancillary for 2010. These data were processed using ArcMap 10.8. As the area changed, the population also changed according to Egypt's population census [61, 62, 63], so we can estimate the population density by using the varied area and population per year.

Depending on the inventory approach, Eq. (1) and statistics are mentioned in Table 2, Table 3, and. Cairo's anthropogenic heat will be calculated in watts per square meter using the methodology shown in Figure 2. The estimation was for the years 2010, 2015 and 2020. The assumed working hours per day was 18 hours.

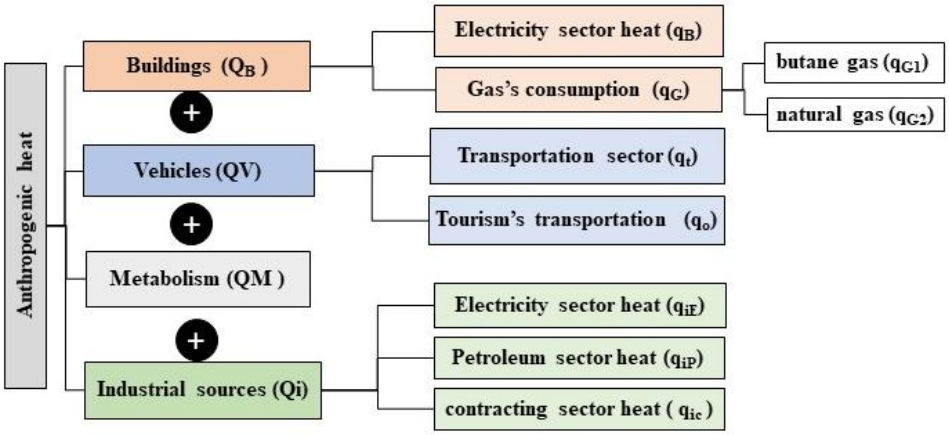

Figure 2. AHF estimation methodology depends on the inventory approach (Authors)

2.2. Anthropogenic Heat Sectors

2.2.1. Buildings

According to annual energy use statistics, the released heat from buildings in Cairo was divided into two types:

Table 2. The data used in estimating AHF is from the building sector

Item	Description	Ref.	Unit	2010	2015	2020
E_P	The consumed electricity, the share per capita	[48]	Kw.h	1786	1941	2057
q_{Gp1}	The share per capita for butane gas	[49]	Ton	0.06	0.05	0.05
q_{Gp2}	The share per capita for natural gas	[50]		0.40	0.39	0.44
C_{E1}	The produced heat from 1 kg of butane gas	[51]	MJ\Kg	45.75		
C_{E2}	The produced heat from 1 kg of natural gas		MJ\Kg	42.54		
PD	The population density for the selected year		per/m^2	Varied for every year		
T	The total time (the year converted to seconds)		S	365*18*60*60		

1. The released heat from electricity (q_E) used in artificial lighting, air conditioning, and other uses depends on the economic level.
2. The released heat from butane gas and natural gas (q_G) consumption was used in cooking activities and heating systems.

So, the emitted heat from the buildings can be estimated by adding the two quantities, following (3).

$$Q_B = q_E + q_G \quad (3)$$

2.2.1.1. Emitted Heat from Electricity (q_E)

The amount of electrical energy consumed in buildings varies from one district to another because of the economic level and population density. According to the annual bulletin of the Egyptian Electricity Holding Company, the consumed electrical energy per capita is estimated from Eq. (4), and the available data is displayed in Table 2.

$$q_E = (PD * E_P)/T(S) \quad (4)$$

2.2.1.2. Emitted Heat from Gases (q_G)

The released heat from gases is divided into two sources:

- The released heat from butane gas (q_{G1}): According to Egypt Oil & Gas [52], 70% of Egyptian households depend on butane cylinders used in residential buildings. So, the released heat from butane gas was estimated depending on Eq. (5) and Table 2.
- The released heat from natural gas (q_{G2}): The available data were the share per capita and the combustion heat for 1 kg of the natural gas so that it can be estimated from Eq. (6) and Table 2.

So, the emitted heat from gases can be estimated by adding the two quantities, following Eq. (7) and Table 2.

$$q_{G1} = (PD * q_{GP1} * C_{E1})/T(S) \quad (5)$$

$$q_{G2} = (PD * q_{GP2} * C_{E2})/T(S) \quad (6)$$

$$q_G = q_{G1} + q_{G2} \quad (7)$$

2.2.2. Vehicles

Quantifying the released heat from vehicles in Cairo is not simple due to the lack of detailed information regarding the varied traffic density with time and heat discharge with vehicle type [22].

Table 3. The available data for estimating the released heat from the vehicle.

Item	Description	Ref	Unit	2010	2015	2020
L_E	Egypt's yearly vehicle count	[53, 54,55]	1000	5853728	8636120	10801239
L_C	Cairo's yearly vehicle count			1851334	2288153	2374328
F_{ET}	Egypt's transport fuel usage	[56, 57, 58]	*	10136	11728	12585
F_{EO}	Egypt's tourism fuel usage		Ton	2711	3739	3793
C_{E3}	The combustion heat for 1 kg of fuel	[51]	MJ/kg	43.4		
PD	The population density		per/m^2	Varied for every year		
T	The total time		S	365*18*60*60		

The available data for assessing the heat discharged from vehicles are mentioned in Table 3. It is assumed to be divided into two quantities. The direct part (FCt) is the heat from transportation; this part could be quantified by applying Eq. (8). The indirect part (FCO) is the heat released from tourism activities. According to the Cairo Governorate Portal, Cairo accounts for 21% of Egypt's tourism. This part could be estimated by applying Eq. (9). So, the heat discharged from vehicles could be estimated by multiplying the total consumed fuel (FCT + FCO) by the fuel consumption heat (CE3), following Eq. (10).

$$F_{Ct} = \left(\frac{L_C}{L_E}\right) * 100 * F_{ET} \quad (8)$$

$$F_{CO} = F_{EO} * 21\% \quad (9)$$

$$Q_v = (F_{CT} + F_{CO}) * \ C_{E3} \quad (10)$$

2.2.3. Metabolism

Due to the high density in Cairo, we could not neglect metabolism [25, 36]. According to FANGER (1970), metabolic rate depends on sex, age, weight, external body surface area, and activity level. It is not easy to quantify Cairo populations according to the last conditions. The heat discharged from humans during the daytime ranges from 115 w to 300 w per person [25]. As reported in most studies, the average metabolic rate for one person standing or doing a light activity during the daytime is 175 w and 70 w during the nighttime [25, 40, 48]. However, few studies used the average of all activities as the average activity level, 171 w [59], and a study in Phoenix used 180 w [60]. This study implies that the average human metabolism is 175 w per person. So, estimating the released heat from Cairo's population [61, 62, 63] (metabolism) follows Eq. (11).

$$Q_M = PD * 175 \quad (11)$$

2.2.4. Industry and Other Sources (Q_i)

The last source of AHF is the released heat from industrial activities, which was collected from three causes:

1. The total consumed electricity in the industrial activities (q_{iE}) was assessed by applying Eq. (12) and Table 4.
2. The released heat from the combustion of petroleum and petrochemical materials (q_{iP}) was estimated by applying Eq. (13) and Table 4.
3. The heat discharged from the contracting and roads sectors (q_{ic}) is the total used fuel in Egypt in contracting and roads and the estimated usage in Cairo, so we can estimate the portion of Cairo from this fuel by following Eq. (14) and Table 4.

The released heat from industry and other sources was assessed depending on the previous results (qiE, qip, qic) and Eq. (15).

$$q_{iE} = \frac{q_{iE\ ALL}}{T(S) * A\ (M2)} \quad (12)$$

$$q_{iP} = \left(PD * \ q_{iP-per} * C_E\ \right)/T(S) \quad (13)$$

$$q_{iC} = \frac{(F_{iC\ all} * \ cf\% * C_E\ )}{T(S) * A(M^2)} \quad (14)$$

$$Q_i = q_{iE} + q_{iP} + q_{iC} \quad (15)$$

Table 4. The available data for estimating the heat discharged from the industrial sector

Item	Description	Ref.	Unit	2010	2015	202
$q_{iE\ all}$	The consumed electricity in industrial activities	[56,	M.Kw.h	4362	5408	474
$F_{iC\ all}$	The consumed fuel in the contracting and roads in Egypt	57,58]	1000	2096	1650	206
$q_{ip\text{-}per}$	The share per capita for petroleum and petrochemicals in Egypt	[48,	*	0.43	0.41	0.33
		49, 50]	Ton			
CF %	The assumed percentage of vehicles in Cairo			32%	26%	26%
C_{E4}	The heat of combustion for 1 kg of fuel	[51]	MJ\KG	44.52		
PD	The population density for the selected year		per/m^2	Varied for every year		
T	The total time (the year converted to seconds)		S	365*18*60*60		
A	Cairo's urban total area		m^2	Varied for every year		

2.3. Estimating the per capita Share (Q_{FP}) and Finding the Hotspots in Cairo (Q_{FD})

AHF per capita was calculated using Eq. (16) and Table 5. Based on the AHF per capita, the AHF per district was assessed to identify hot spots in the study area using Eq. (17) and Table 5.

Table 5. The available data for estimating the per capita share and hotspots.

Item	Description	Unit	2010	2015	2020
A	Cairo's urban total area	m^2	Varied for every year		
A_D	District total area	m^2	Varied for every district		
Q_F	The estimated AHF in 2015	w/m^2	24.5		
P	Cairo's total population in 2015	Person	9278441		

$$Q_{FP} = \frac{A\ * Q_F}{P} \quad \text{(w/per)} \quad (16)$$

$$Q_{FD} = Q_{FP} * A_D \quad \text{(w/m}^2\text{)} \quad (17)$$

2.4. Experiment Limitations

Given the lack of accessible data for Cairo, the study made the following assumptions:

Building sector: Although there is no data about the electricity consumed in every district, given the different economic levels in Cairo's districts, the study assumed that the consumption rates were equal for all districts.

Vehicles sector:

1. Due to the lack of detailed data on traffic densities and vehicle types, the study relied on Cairo's total gasoline quantity and usage ratio.
2. There are no data on the differences between natural gas and gasoline types (such as 95, 92 and 80); consequently, the study assumed that the heat composition of gasoline remains fixed and does not vary.

Metabolism sector: The study assumed a constant metabolic rate due to the population filtering challenges. However, the metabolic rate differs by gender, age, activity and clothing level.

Industrial sector: the data used for 2020 were estimated from 2019 due to the lack of data. for 2020 were estimated from 2019 due to the lack of data.

3. Results and Discussion

3.1. Detect the Changes in Urban Area

Depending on the satellite images, Landsat 8 (OLI), bands 1 to 7 for 2015 and 2020, and Landsat 7 (ETM+) for 2010, the changes in the urban area in Cairo (buildings, roads, cultivated lands, and water surfaces) were detected throughout the period of this period (Figure 3a-3c). The official borders of Cairo governorate's total area (using ArcMap 10.8 and satellite images) are approximately 2753.9 km^2.

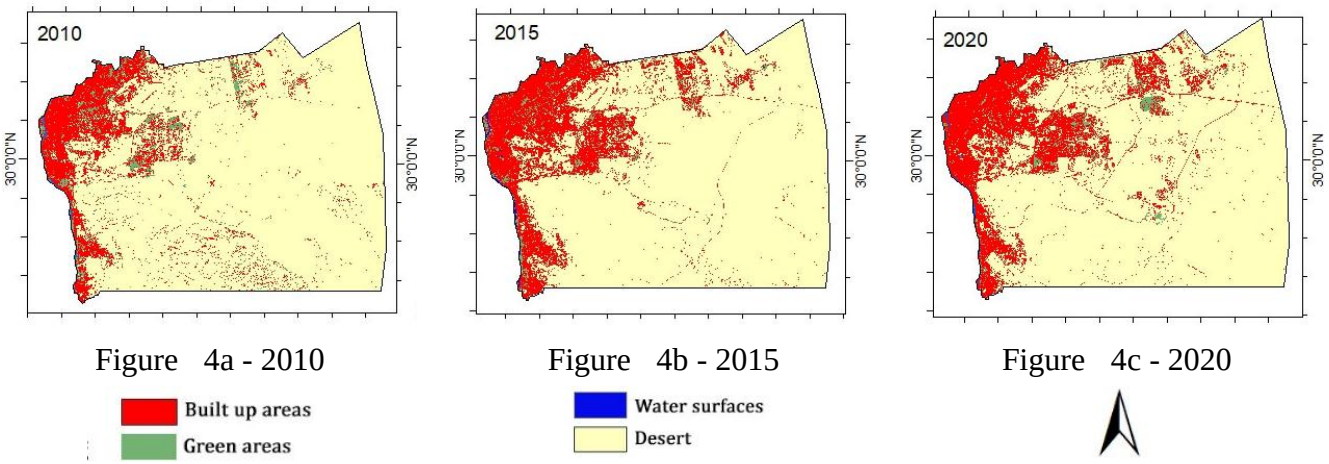

Figure 4a - 2010 Figure 4b - 2015 Figure 4c - 2020

Figure 3. Landsat images showing Cairo's urban area (Authors)

The urban mass area grew rapidly from 2010 to 2015, and the assigned area increased by approximately 155.5 km^2 and increased from 2015 to 2020 by 30.2 km^2, which was less than the previous increase. The difference in area increased by 125.5 km^2 between the two periods (Figure 4a-4c). This decrease in urban growth was due to planning and economic reasons:

- Changes in the building permit laws and freezes in new construction permits for some periods.
- The rapid change in the Egyptian economy changed the mindset towards investing money.
- The sharp rise in building material prices.

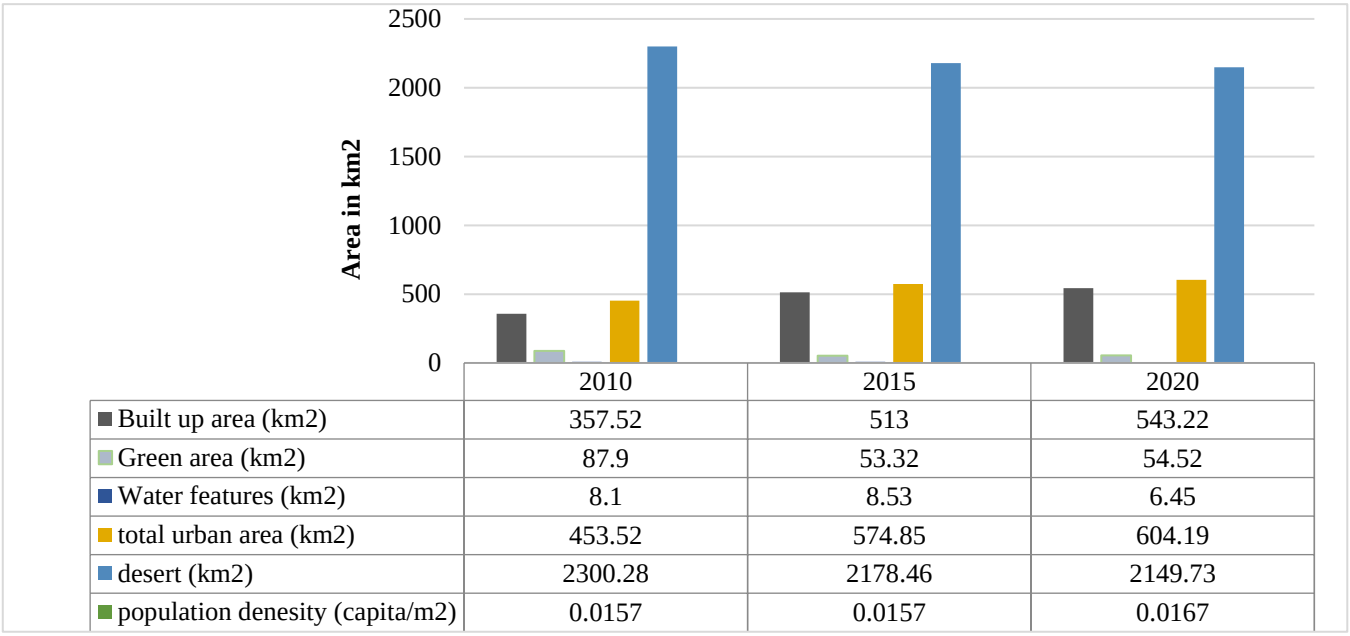

	2010	2015	2020
Built up area (km2)	357.52	513	543.22
Green area (km2)	87.9	53.32	54.52
Water features (km2)	8.1	8.53	6.45
total urban area (km2)	453.52	574.85	604.19
desert (km2)	2300.28	2178.46	2149.73
population denesity (capita/m2)	0.0157	0.0157	0.0167

Figure 4. Cairo's total urban area and population density in 2010, 2015 and 2020 (Authors)

The cultivated land (Figure 4) decreased by 34.6 km^2 from 2010 to 2015; the reduction exceeded that of the 2015 to 2020 period, which was 1 km^2. Water surfaces in Cairo (the Nile River and some water surfaces in clubs and compounds) formed the smallest part of the total area, which increased by less than 0.5 km^2 from 2010 to 2015 but decreased by about 2 km^2 from 2015 to 2020. The total area of the desert decreased by about 122 km^2 from 2010 to 2015 and 28.7 km^2 from 2015 to 2020.

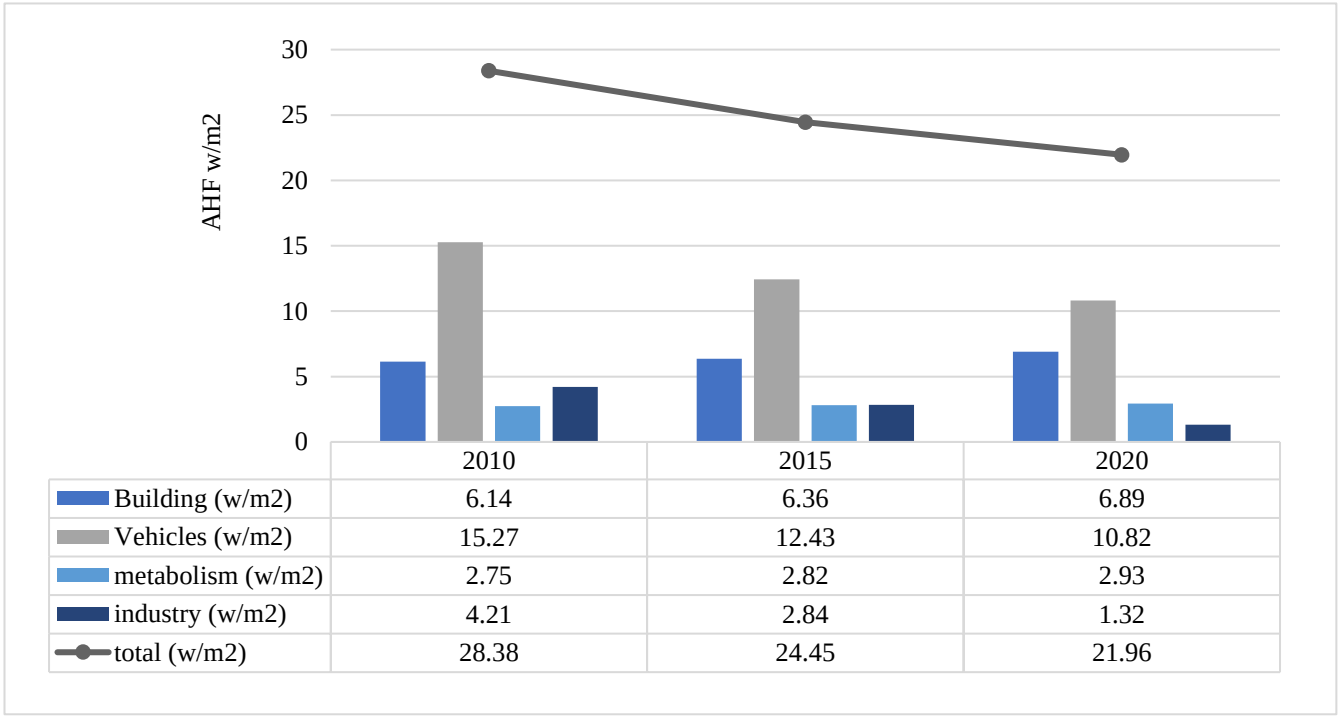

	2010	2015	2020
Building (w/m2)	6.14	6.36	6.89
Vehicles (w/m2)	15.27	12.43	10.82
metabolism (w/m2)	2.75	2.82	2.93
industry (w/m2)	4.21	2.84	1.32
total (w/m2)	28.38	24.45	21.96

Figure 5. The total anthropogenic heat in Cairo (w/m^2) and each sector's participation rate (Authors)

Depending on the inventory approach, the average and the share per capita of AHF in Cairo were estimated and detailed in Figure 5. The average AHF decreased by about 13.7% (4 w/m^2) from 2010 to 2015 and 10.2% (2.5 w/m^2) from 2015 to 2020. The magnitude of AHF in megacities has been discussed in several studies. AHF in megacities ranged between 20 and 160 w/m^2 [64]. AHF's rate for any city was less than 100 w/m^2 [62, 66]. The per capita share of AHF also decreased by about 16.5% (288.5 w) from 2010 to 2015 and 13.2% (201.2 w) from 2015 to 2020.

Analysis of the total AHF results for Cairo and other megacities and studies showed that the magnitude of AHF in Cairo is the lowest among other cities; however, the population density in Cairo is the highest, as shown in Table 6. In addition, AHF increased over the years because of the population increase [38, 62, 63], but in Cairo, it decreased over the study period for the following reasons:

Table 6. AHF Magnitudes of Various Urban City Centres Compared to Cairo

City	Population density capita/km^2	Year	Mean AHF w/m^2	Ref.
Beijing	2437.46	2012	87	[19]
Mexico City	64.91	Average of the last 50 years	24.7	[67]
London	5666.72	2010	20	[68]
Tokyo	6399	1995	400	[29]
Singapore	8262.17	2008	23.5	[30]
Los Angeles	2994.08	2000	15	[24]
San Francisco	1455.17	2000	58.75	[24]
Chicago	4528.82	2000	58.75	[24]
Manchester	4737.26	2003	16.5	[22]
Cairo	15,700	2015	24.5	Present study

- According to the World Bank database, Egypt's GDP per capita growth decreased. It was 3%, 2.1%, and 1.8 % in 2010, 2015 and 2020, respectively, so if the GDP per capita growth remains constant from 2010 to 2020, AHF would be more than the current results by 40%.
- According to the World Factbook 2016, the global average energy consumption was 2,674 kWh/capita per year, and the average of the consumed energy in Egypt was 1,510 kWh/capita per year, so the per capita energy in Egypt reached approximately half of the global energy share (56%), so AHF will be raised approximately 43%.
- Consumer prices rose, which led to the rationalizing of electricity consumption in government and private buildings and reduced street lighting [72].
- There was an increase in the use of renewable energy sources such as solar and wind energy [73].

The second cause was the buildings, which formed approximately 20%, 26% and 30% in 2010, 2015 and 2020, respectively, of Cairo's AHF (Figure 5). Buildings' AHF increased by 4% (0.26 w/m^2) from 2010

to 2015 and 7.2% (0.5 w/m^2) from 2015 to 2020. According to most research, buildings are the main cause of AHF. In Singapore [59], the buildings contributed 49%–82% and 46%–81% during work and off days, respectively. In Manchester [22], the buildings contributed 60% of the city's AHF.

AHF from vehicles formed more than half of the total AHF, which formed approximately 54%, 51% and 50% of total AHF in 2010, 2015 and 2020, respectively (Figure 5). The vehicles' AHF decreased by 18.9% (2.9 w/m^2) from 2010 to 2015 and 12.9% (1.6 w/m^2) from 2015 to 2020. In the majority of studies [69], AHF increased over time. This decrease in consumed fuel was 3774.980 in 2010 and 3562.923 tons in 2020, according to CAPMAS. This decrease could be attributed to the recent increases in fuel prices, which have been raised more than five times from 2014 until now [74]. So, despite the increased number of licensed vehicles [56–58], the emitted heat from vehicles decreased.

AHF from human metabolism was a less important cause, which formed 10%, 12% and 14% of total AHF in 2010, 2015 and 2020, respectively (Figure 5). The metabolism's AHF increase was insignificant, which ranged from 0.05 to 0.1 w/m^2. In most studies, metabolism was overlooked [75], but in the Cairo urban area, we could not neglect it because of the high population density in the study area.

AHF from industrial activities formed 15%, 11% and 6% of total AHF in 2010, 2015 and 2020, respectively (Figure 5). The industrial AHF decreased by 0.33% (1.4 w/m^2) from 2010 to 2015 and by 53.5% (1.5 w/m^2). Most studies ignored the industry sector because it is located outside the urban area. The industrial activities in Cairo were distributed among small workshops and factories in urban areas like Helwan and 15th of May City.

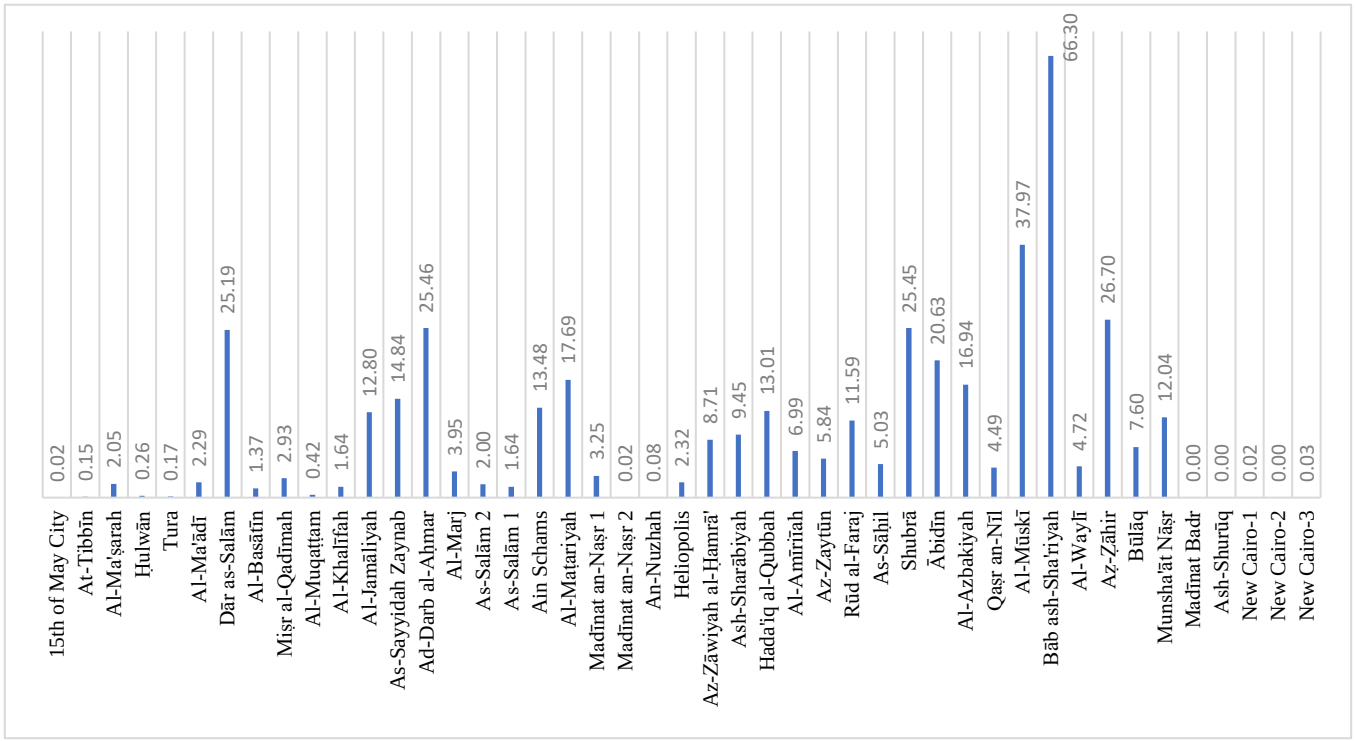

Figure 6. The spatial distribution of the anthropogenic heat in Cairo's districts (Authors)

3.2. The Spatial Distribution of AHF (Hotspots) according to Population Density

AHF distributed evenly in Section 2.2 did not reflect the actual distribution. Several studies have found that AHF is directly proportional to population density [40]. In Figure 6, the actual density distribution for Cairo in 2017 reflects the actual distribution for AHF in Cairo (considering that the per capita share of AHF was equal to the calculated value in 2015, 1514.68 w/m^2).

The results show that the hotspots were located in Bāb ash-Sha'riyah and Al-Mūskī, which were 66.30 w/m^2 and 37.97 w/m^2, respectively. AHF amounts in several districts were near the average estimation, such as Aẓ-Ẓāhir, Ad-Drab al-Aḥmar, Shubrā, and Dār as-Salām, which were 26.7, 25.46, 25.45 and 25.19 w/m^2, respectively. The lowest amount of AHF was located in the new districts, such as New Cairo 1, 2 and 3.

4. Conclusion

Depending on the inventory approach, AHF in Cairo (per meter square and per capita) was estimated in 2010, 2015, and 2020 (Figure 5) to provide an updated and better image of the AHF pattern in Cairo. The AHF sources were estimated: vehicles were the main source, followed by buildings, and the least significant sources were metabolism and industry. Depending on the districts' population density, the hotspots were detected in Bāb ash-Sha'riyah and Al-Mūskī (Figure 6).

The decline in AHF for 2015 and 2020 comes back to the decline in GDP and the average per capita share in Egypt, which was less than the per capita global share average. AHF averages will be raised by 40%–43% in the event of moderate economic conditions for the country.

Understanding AHF patterns and the weight of the various causes is crucial for urban planning to manage AHF hotspots, for health to maximize thermal comfort impacts, and for future-proofing interventions to reduce AHF. Planning tools like Urban Climatic and Climatope Maps should include AHF pattern data. These maps visualize assessments to aid planners, developers and policymakers make better mitigation and adaptation decisions.

Declaration of Competing Interest: The authors declare they have no known competing interests.

References

[1] L. Howard, *The Climate of London: Deduced from Meteorological Observations*. 2013. doi: 10.1017/CBO9781139226899.

[2] S. M. Kareem and H. K. Abdullah, "Effects of Urban Green Space's Physical Features on the Usability of Investment Housing Projects in Erbil City," *Journal of Studies in Science and Engineering*, vol. 3, no. 2, pp. 14-36, 2023.

[3] A. J. Arnfield, "Two decades of urban climate research: A review of turbulence, exchanges of energy and water, and the urban heat island," *Int. J. Climatol.*, vol. 23, no. 1, pp. 1–26, 2003, doi: 10.1002/joc.859.

[4] V. Masson, A. Lemonsu, J. Hidalgo, and J. Voogt, "Urban climates and climate change," *Annu. Rev. Environ. Resour.*, vol. 45, pp. 411–444, 2020, doi: 10.1146/annurev-environ-012320-083623.

[5] J. A. Voogt and T. R. Oke, "Thermal remote sensing of urban climates," *Remote Sens. Environ.*, vol. 86, no. 3, pp. 370–384, 2003, doi: 10.1016/S0034-4257(03)00079-8.

[6] A. Cecilia, G. Casasanta, I. Petenko, A. Conidi, and S. Argentini, "Measuring the urban heat island of Rome through a dense weather station network and remote sensing imperviousness data," *Urban Clim.*, vol. 47, no. September 2022, p. 101355, 2023, doi: 10.1016/j.uclim.2022.101355.

[7] X. Deng, F. Gao, S. Liao, Y. Liu, and W. Chen, "Spatiotemporal evolution patterns of urban heat island and its relationship with urbanization in Guangdong-Hong Kong-Macao greater bay area of China from 2000 to 2020," *Ecol. Indic.*, vol. 146, no. September 2022, p. 109817, 2023, doi: 10.1016/j.ecolind.2022.109817.

[8] S. Tesfamariam, V. Govindu, and A. Uncha, "Spatio-temporal analysis of urban heat island (UHI) and its effect on urban ecology: The case of Mekelle city, Northern Ethiopia," *Heliyon*, vol. 9, no. 2, p. e13098, 2023, doi: 10.1016/j.heliyon.2023.e13098.

[9] H. Hou *et al.*, "Driving forces of UHI changes in China's major cities from the perspective of land surface energy balance," *Sci. Total Environ.*, vol. 829, p. 154710, 2022, doi: 10.1016/j.scitotenv.2022.154710.

[10] S. Barrao, R. Serrano-Notivoli, J. M. Cuadrat, E. Tejedor, and M. A. Saz Sánchez, "Characterization of the UHI in Zaragoza (Spain) using a quality-controlled hourly sensor-based urban climate network," *Urban Clim.*, vol. 44, 2022, doi: 10.1016/j.uclim.2022.101207.

[11] H. Louiza, A. Zéroual, and H. Djamel, "Impact of the Transport on the Urban Heat Island," *Int. J. Traffic Transp. Eng.*, vol. 5, no. 3, pp. 252–263, 2015, doi: 10.7708/ijtte.2015.5(3).03.

[12] H. Ashraf, T. A. El Seoud, S. Sodoudi, and A. El Zafarany, "Anisotropic Surface Urban Heat Island in Cairo, Egypt: A Spatiotemporal Analysis of Local Climate Change from 2000 to 2021," *Civ. Eng. Archit.*, vol. 11, no. 1, pp. 331–350, 2023, doi: 10.13189/cea.2023.110127.

[13] W. O. Library and D. J. Sailor, "A review of methods for estimating anthropogenic heat and moisture emissions in the urban environment," *Int. J. Climatol. Int. J. Clim.*, vol. 31, pp. 189–199, 2011, doi: 10.1002/joc.2106.

[14] J. Qian, Q. Meng, L. Zhang, D. Hu, X. Hu, and W. Liu, "Improved anthropogenic heat flux model for fine spatiotemporal information in Southeast China," *Environ. Pollut.*, vol. 299, no. November 2021, p. 118917, 2022, doi: 10.1016/j.envpol.2022.118917.

[15] W. granett, a; bach, "an estimation of the ratio of artificial heat generation to natural radiation heat in sheffield," *Weather note*, 1965.

[16] Y. Chen, W. M. Jiang, N. Zhang, X. F. He, and R. W. Zhou, "Numerical simulation of the anthropogenic heat effect on urban boundary layer structure," *Theor. Appl. Climatol.*, vol. 97, no. 1–2, pp. 123–134, 2009, doi: 10.1007/s00704-008-0054-0.

[17] C. Park, N. D. Werner, D. J. Sailor, and C. Kim, "SC," 2015.

[18] L. Allen, F. Lindberg, and C. S. B. Grimmond, "Global to city scale urban anthropogenic heat flux: Model and variability," *Int. J. Climatol.*, vol. 31, no. 13, pp. 1990–2005, 2011, doi: 10.1002/joc.2210.

[19] R. Sun, Y. Wang, and L. Chen, "A distributed model for quantifying temporal-spatial patterns of anthropogenic heat based on energy consumption," *J. Clean. Prod.*, vol. 170, pp. 601–609, 2018, doi: 10.1016/j.jclepro.2017.09.153.

[20] V. K. Singh, S. Bhati, M. Mohan, N. R. Sahoo, and S. Dash, "Numerical simulation of the impact of urban canopies and anthropogenic emissions on heat island effect in an industrial area: A case study of Angul-Talcher region in India," *Atmos. Res.*, vol. 277, no. June, p. 106320, 2022, doi: 10.1016/j.atmosres.2022.106320.

[21] G. Pigeon, D. Legain, P. Durand, and V. Masson, "Anthropogenic heat release in an old European agglomeration (Toulouse, France)," *Int. J. Climatol.*, vol. 27, pp. 1969–1981, 2007, doi: 10.1002/joc.1530.

[22] C. Smith, S. Lindley, and G. Levermore, "Estimating spatial and temporal patterns of urban anthropogenic heat fluxes for UK cities: The case of Manchester," *Theor. Appl. Climatol.*, vol. 98, no. 1–2, pp. 19–35, 2009, doi: 10.1007/s00704-008-

0086-5.

[23] M. Iamarino, S. Beevers, and C. S. B. Grimmond, "High-resolution (space, time) anthropogenic heat emissions: London 1970-2025," *Int. J. Climatol.*, vol. 32, no. 11, pp. 1754–1767, 2012, doi: 10.1002/joc.2390.

[24] D. J. Sailor and L. Lu, "A top-down methodology for developing diurnal and seasonal anthropogenic heating profiles for urban areas," *Atmos. Environ.*, vol. 38, no. 17, pp. 2737–2748, 2004, doi: 10.1016/j.atmosenv.2004.01.034.

[25] Y. Dong, A. C. G. Varquez, and M. Kanda, "Global anthropogenic heat flux database with high spatial resolution," *Atmos. Environ.*, vol. 150, pp. 276–294, 2017, doi: 10.1016/j.atmosenv.2016.11.040.

[26] W. He, X. X. Li, X. Zhang, T. Yin, L. K. Norford, and C. Yuan, "Estimation of anthropogenic heat from buildings based on various data sources in Singapore," *Urban Clim.*, vol. 49, no. August 2022, p. 101434, 2023, doi: 10.1016/j.uclim.2023.101434.

[27] Y. Ohashi, Y. Genchi, H. Kondo, Y. Kikegawa, H. Yoshikado, and Y. Hirano, "Influence of air-conditioning waste heat on air temperature in Tokyo during summer: Numerical experiments using an urban canopy model coupled with a building energy model," *J. Appl. Meteorol. Climatol.*, vol. 46, no. 1, pp. 66–81, 2007, doi: 10.1175/JAM2441.1.

[28] K. Klysik, "SPATIAL AND SEASONAL DISTRIBUTION OF ANTHROPOGENIC HEAT EMISSIONS IN LODZ, POLAND," *Atmospheric" Environment*, vol. 30, no. 20. pp. 3397–3404, 1996.

[29] T. Ichinose, K. Shimodozono, and K. Hanaki, "Impact of anthropogenic heat on urban climate in Tokyo," *Atmos. Environ.*, vol. 33, no. 24–25, pp. 3897–3909, 1999, doi: 10.1016/S1352-2310(99)00132-6.

[30] P. Boehme, M. Berger, and T. Massier, "Estimating the building based energy consumption as an anthropogenic contribution to urban heat islands," *Sustain. Cities Soc.*, vol. 19, pp. 373–384, 2015, doi: 10.1016/j.scs.2015.05.006.

[31] S.-H. Lee and S.-T. Kim, "Estimation of Anthropogenic Heat Emission over South Korea Using a Statistical Regression Method," *J. Atmos. Sci*, vol. 51, no. 2, pp. 1976–7633, 2015, doi: 10.1007/s13143-015-0065-6.

[32] M. Iamarino, S. Beevers, and C. S. B. Grimmond, "High-resolution (space, time) anthropogenic heat emissions: London 1970-2025," *Int. J. Climatol.*, vol. 32, no. 11, pp. 1754–1767, 2012, doi: 10.1002/joc.2390.

[33] D. Sailor, "Anthropogenic Heat and Moisture Emissions in the Urban Environment," *Seventh Int. Conf. Urban Clim. …*, no. July, 2009, [Online]. Available: http://www.ide.titech.ac.jp/~icuc7/extended_abstracts/pdf/sailor_extended_abstract_ICUC7.pdf

[34] Y. Zhang, H. Balzter, and X. Wu, "Spatial-temporal patterns of urban anthropogenic heat discharge in China observed from sensible heat flux using Landsat TM/ETM+ data 2 3."

[35] S. Wang, D. Hu, S. Chen, and C. Yu, "A partition modeling for anthropogenic heat flux mapping in China," *Remote Sens.*, vol. 11, no. 9, pp. 1–18, 2019, doi: 10.3390/rs11091132.

[36] A. Block, K. Keuler, and E. Schaller, "Impacts of anthropogenic heat on regional climate patterns," 2004, doi: 10.1029/2004GL019852.

[37] Y. Zheng and Q. Weng, "High spatial- and temporal-resolution anthropogenic heat discharge estimation in Los Angeles County, California," *J. Environ. Manage.*, vol. 206, pp. 1274–1286, 2018, doi: 10.1016/j.jenvman.2017.07.047.

[38] F. Lindberg, C. S. B. Grimmond, N. Yogeswaran, S. Kotthaus, and L. Allen, "Impact of city changes and weather on anthropogenic heat flux in Europe 1995-2015," *Urban Clim.*, vol. 4, no. 2013, pp. 1–15, 2013, doi: 10.1016/j.uclim.2013.03.002.

[39] Y. Chen, W. M. Jiang, N. Zhang, X. F. He, and R. W. Zhou, "Numerical simulation of the anthropogenic heat effect on urban boundary layer structure," *Theor. Appl. Climatol.*, vol. 97, no. 1–2, pp. 123–134, 2009, doi: 10.1007/s00704-008-0054-0.

[40] C. A. Kennedy *et al.*, "Energy and material flows of megacities," *Proc. Natl. Acad. Sci. U. S. A.*, vol. 112, no. 19, pp. 5985–5990, 2015, doi: 10.1073/pnas.1504315112.

[41] H. A. Effat and O. A. K. Hassan, "Change detection of urban heat islands and some related parameters using multi-

temporal Landsat images; a case study for Cairo city, Egypt," *Urban Clim.*, vol. 10, no. P1, pp. 171–188, 2014, doi: 10.1016/j.uclim.2014.10.011.

[42] M. El-Hattab, S. M. Amany, and G. E. Lamia, "Monitoring and assessment of urban heat islands over the Southern region of Cairo Governorate, Egypt," *Egypt. J. Remote Sens. Sp. Sci.*, vol. 21, no. 3, pp. 311–323, 2018, doi: 10.1016/j.ejrs.2017.08.008.

[43] I. A. El-Magd, A. Ismail, and N. Zanaty, "Spatial Variability of Urban Heat Islands in Cairo City, Egypt using Time Series of Landsat Satellite Images," *Int. J. Adv. Remote Sens. GIS*, vol. 5, no. 1, pp. 1618–1638, 2016, doi: 10.23953/cloud.ijarsg.48.

[44] W. T. L. Chow, F. Salamanca, M. Georgescu, A. Mahalov, J. M. Milne, and B. L. Ruddell, "A multi-method and multi-scale approach for estimating city-wide anthropogenic heat fluxes," *Atmos. Environ.*, vol. 99, pp. 64–76, 2014, doi: 10.1016/j.atmosenv.2014.09.053.

[45] D. J. Sailor and L. Lu, "A top-down methodology for developing diurnal and seasonal anthropogenic heating profiles for urban areas," *Atmos. Environ.*, vol. 38, no. 17, pp. 2737–2748, 2004, doi: 10.1016/j.atmosenv.2004.01.034.

[46] D. Athukorala and Y. Murayama, "Urban heat island formation in greater Cairo: Spatio-temporal analysis of daytime and nighttime land surface temperatures along the urban-rural gradient," *Remote Sens.*, vol. 13, no. 7, 2021, doi: 10.3390/rs13071396.

[47] N. Girgis, S. Elariane, and M. A. Elrazik, "Evaluation of heat exhausts impacts on pedestrian thermal comfort," *Sustain. Cities Soc.*, vol. 27, pp. 152–159, 2016, doi: 10.1016/j.scs.2015.06.010.

[48] Central Agency for Public Mobilization & Statistics (CAPMAS), "Annual Bulletin of Electricity and Energy Statistics for the year 2009/2010," Cairo, 2011.

[49] C. A. for P. M. & S. (CAPMAS), "Annual Bulletin of Electricity and Energy Statistics for the year 2015/2014," Cairo, 2016.

[50] C. A. for P. M. & S. (CAPMAS), "Annual Bulletin of Electricity and Energy Statistics for the year 2017/2016," Cairo, 2018.

[51] R. A. Fletcher and G. Pilcher, "Measurements of heats of combustion by flame calorimetry. Part 8.—Methane, ethane, propane, n-butane and 2-methylpropane," *Trans. Faraday Soc.*, vol. 66, pp. 794–799, 1970, doi: 10.1039/TF9706600794.

[52] B. M. Samir and R. Hossam, "Were Subsidy Cuts the Main Driver Behind the Fall of Butane Cylinders' Consumption ?," pp. 1–5, 2017.

[53] C. A. for P. M. & S. (CAPMAS), "Bulletin of Licensed Vehicles Statistics 2010," Cairo, 2012. [Online]. Available: https://www.capmas.gov.eg/Pages/Publications.aspx?page_id=5104&Year=23566

[54] C. A. for P. M. & S. (CAPMAS), "Bulletin of licensed Vehicles statistics in 31/12/2015," Cairo, 2016.

[55] C. A. for P. M. & S. (CAPMAS), "Bulletin of licensed Vehicles statistics in 31/12/2020," Cairo, 2021.

[56] C. A. for P. M. & S. (CAPMAS), "Annual Bulletin of Environment Statistics 2010," Cairo, 2011.

[57] C. A. for P. M. & S. (CAPMAS), "Annual Bulletin of Environment Statistics 2015," Cairo, 2017. [Online]. Available: http://www.capmas.gov.eg

[58] C. A. for P. M. & S. (CAPMAS), "Annual Bulletin of Environment Statistics 2017," Cairo, 2017. [Online]. Available: http://www.capmas.gov.eg

[59] A. K. L. Quah and M. Roth, "Diurnal and weekly variation of anthropogenic heat emissions in a tropical city, Singapore," *Atmos. Environ.*, vol. 46, pp. 92–103, 2012, doi: 10.1016/j.atmosenv.2011.10.015.

[60] W. T. L. Chow, F. Salamanca, M. Georgescu, A. Mahalov, J. M. Milne, and B. L. Ruddell, "A multi-method and multi-scale approach for estimating city-wide anthropogenic heat fluxes," *Atmos. Environ.*, vol. 99, pp. 64–76, 2014, doi: 10.1016/j.atmosenv.2014.09.053.

[61] C. A. for P. M. & S. (CAPMAS), "Egypt in Figures 2010," Cairo, 2010. [Online]. Available:

https://www.sis.gov.eg/Story/129692/Egypt-in-Figures-2018?lang=en-us

[62] C. A. for P. M. & S. (CAPMAS), "Egypt in Figures 2015," Cairo, 2015. [Online]. Available: https://www.sis.gov.eg/Story/129692/Egypt-in-Figures-2018?lang=en-us

[63] CAPMAS, "Egypt in Figures 2020," 2022. [Online]. Available: https://www.capmas.gov.eg/Pages/StaticPages.aspx?page_id=5035

[64] T. R. Oke, "The urban energy balance," *Prog. Phys. Geogr.*, vol. 12, no. 4, pp. 471–508, 1988, doi: 10.1177/030913338801200401.

[65] K. Klysik, "SPATIAL AND SEASONAL DISTRIBUTION OF ANTHROPOGENIC HEAT EMISSIONS IN LODZ, POLAND," 1996.

[66] F. Kimura and S. Takahashi, "The effects of land-use and anthropogenic heating on the surface temperature in the Tokyo Metropolitan area: A numerical experiment," *Atmos. Environ. Part B, Urban Atmos.*, vol. 25, no. 2, pp. 155–164, 1991, doi: 10.1016/0957-1272(91)90050-O.

[67] M. Bonifacio-Bautista, M. Ballinas, A. Jazcilevich, and V. L. Barradas, "Estimation of anthropogenic heat release in Mexico City," *Urban Clim.*, vol. 43, no. August 2021, p. 101158, 2022, doi: 10.1016/j.uclim.2022.101158.

[68] M. Iamarino, S. Beevers, and C. S. B. Grimmond, "High-resolution (space, time) anthropogenic heat emissions: London 1970-2025," *Int. J. Climatol.*, vol. 32, no. 11, pp. 1754–1767, 2012, doi: 10.1002/joc.2390.

[69] S. Ziaul and S. Pal, "Anthropogenic heat flux in English Bazar town and its surroundings in West Bengal, India," *Remote Sens. Appl. Soc. Environ.*, vol. 11, no. June, pp. 151–160, 2018, doi: 10.1016/j.rsase.2018.06.003.

[70] S. Chen *et al.*, "Characterizing spatiotemporal dynamics of anthropogenic heat fluxes: A 20-year case study in Beijing–Tianjin–Hebei region in China," *Environ. Pollut.*, vol. 249, pp. 923–931, 2019, doi: 10.1016/j.envpol.2019.03.113.

[71] B. Chen *et al.*, "Anthropogenic heat release due to energy consumption exacerbates European summer extreme high temperature," *Clim. Dyn.*, vol. 61, no. 7–8, pp. 3831–3843, 2023, doi: 10.1007/s00382-023-06775-x.

[72] H. Ritchie and M. Roser, "Australia : Energy Country Profile Access to energy," pp. 1–27, 2022, [Online]. Available: https://ourworldindata.org/energy/country/australia?country=AUS~DEU~IND~GBR

[73] Arabic Egyptian Electricity Holding Company, "Arabic Egyptian Electricity Holding Company Annaul Report 2017-2018," Cairo, 2020.

[74] I. Shaarawy, "Egypt raises fuel prices," pp. 5–8, 2023, [Online]. Available: https://egyptoil-gas.com/news/egypt-raises-fuel-prices/

[75] D. J. Sailor, M. Georgescu, J. M. Milne, and M. A. Hart, "Development of a national anthropogenic heating database with an extrapolation for international cities," *Atmos. Environ.*, vol. 118, pp. 7–18, 2015, doi: 10.1016/j.atmosenv.2015.07.016.